*Eur. J. Mech. B - Fluids 20 (2001) 557–576*

S0997-7546(01)01130-X/FLA

# Two-dimensional turbulence in square and circular domains with no-slip walls

H.J.H. Clercx [a,*], A.H. Nielsen [b], D.J. Torres [c], E.A. Coutsias [d]

[a] *Department of Physics, Eindhoven University of Technology, P.O. Box 513, NL-5600 MB Eindhoven, The Netherlands*
[b] *Optics and Fluid Dynamics Department, Forskningscenter Risø, DK-4000 Roskilde, Denmark*
[c] *Physics Department and Geophysical Research Center, New Mexico Tech, Socorro, NM 87801, USA*
[d] *Department of Mathematics and Statistics, University of New Mexico, Albuquerque, NM 87131, USA*

(Received 10 April 2000; accepted 20 July 2000)

**Abstract** – Several fascinating phenomena observed for 2D turbulence in bounded domains are discussed. The first part of this paper concerns a short overview of the non-trivial behaviour of freely evolving 2D turbulence in square domains with no-slip boundaries. In particular, the Reynolds number dependence of, and the influence of the initial conditions on spontaneous spin-up of the flow, which is characterised by a sudden increase of the absolute value of the angular momentum of the flow, is investigated in more detail. In a second set-up we have investigated forced 2D turbulence in circular containers with no-slip walls. A comparison with the double periodic case reveals that domain-filling structures, always observed in the double periodic cases, are being prevented from emerging. Wall-generated, small-scale structures are continuously injected into the interior of the domain, destroying larger structures and maintaining the turbulent flow field. © 2001 Éditions scientifiques et médicales Elsevier SAS

**2D turbulence / energy spectra / spontaneous spin-up / angular momentum / spectral methods**

## 1. Introduction

In this paper we discuss several interesting phenomena for decaying and forced 2D turbulence in bounded domains with no-slip boundary conditions. The first part concerns decaying 2D turbulence and the surprising phenomenon of spontaneous spin-up of the flow during the decay process. In the second part a few examples of forced 2D turbulence in a circular domain with a no-slip wall will be discussed in order to show that also for forced 2D turbulence the presence of no-slip boundaries will modify the time evolution of the flow dramatically. In section 2 a short overview of theoretical and numerical aspects of 2D turbulence is presented, and in section 3 a short overview of the numerical method to simulate decaying 2D turbulence in bounded square domains is given. Additionally, the different initialisation procedures of the flow are presented there. The role of initial conditions and Reynolds number dependence on the spin-up process is discussed in more detail in section 4. Results of forced 2D turbulence in a bounded circular domain are presented in section 5, and the main results of this paper are summarised in section 6.

## 2. Decaying 2D turbulence in square domains with no-slip walls

During the last decades many theoretical and numerical studies have been carried out to improve the understanding of two-dimensional (2D) turbulence. [1] Thirty years ago the first phenomenological theory of

* Correspondence and reprints.
*E-mail address:* h.j.h.clercx@tue.nl (H.J.H. Clercx).

[1] For a more comprehensive overview of the developments in the field of 2D turbulence until 1980 we refer to a survey on hydrodynamic and plasma applications by Kraichnan and Montgomery [1].

forced 2D turbulence was presented by Kraichnan [2] and by Batchelor [3]. According to this theory, the energy spectrum shows an inverse energy cascade with a $k^{-5/3}$ inertial range for wave numbers smaller than the wave number $k_i$ associated with the injection scale of the forcing (i.e. $k < k_i$). A direct enstrophy cascade, characterised by a $k^{-3}$ inertial range, is predicted for $k > k_i$. Numerical studies of forced 2D turbulence with periodic boundary conditions more or less support the Kraichnan–Batchelor picture [4–7], although steeper spectra for large wave numbers are also observed [6]. The energy spectra obtained for numerical simulations of decaying 2D turbulence with periodic boundaries show that the inverse cascade is usually not very clearly observed, and the direct enstrophy cascade is often only established as a transient state before the viscous range starts to dominate the large wave number spectrum [8,9]. Additionally, the appearance of coherent vortices during the decay process introduces steeper spectra for large wave numbers than predicted by Kraichnan and Batchelor. It is assumed that due to the presence of a hierarchy of coherent vortices the energy spectrum becomes more steep [8].

The emergence and the temporal evolution of a hierarchy of coherent vortices in decaying 2D turbulence has been subject to many analytical, numerical and experimental studies [10–18]. An interesting theoretical result is the scaling theory as put forward by Carnevale et al. [14,15]. They assumed that the total kinetic energy $E$ of the flow and the vorticity extremum $\omega_{ext}$ of the dominant vortices are conserved in freely evolving 2D turbulence. It is also supposed that the average number density of vortices decreases algebraically: $\rho(t) \propto t^{-\zeta}$, with $\zeta$ so far undetermined. Dimensional analysis then yields for the average number density $\rho(t) \propto L^{-2}(t/T)^{-\zeta}$, the average enstrophy $Z(t) \propto T^{-2}(t/T)^{-\zeta/2}$, the average vortex radius $a(t) \propto L(t/T)^{\zeta/4}$ and the average mean vortex separation $r(t) \propto L(t/T)^{\zeta/2}$. The characteristic length scale $L$ and time scale $T$ are defined by $L = \omega_{ext}^{-1}\sqrt{E}$ and $T = \omega_{ext}^{-1}$, respectively. The power-law exponent is a free parameter which has to be predicted on the basis of numerical simulations. Computations with a simple, punctuated-Hamiltonian, dynamical model for the evolution of a system of coherent vortices [14] and also numerical simulations of the Navier–Stokes equations, although hyperviscosity has been used, show that $\zeta$ is approximately $0.72 \pm 0.03$ [18]. Measurements of the evolution of several vortex properties, such as vortex density, vortex radius etc., have been performed recently in experiments of decaying 2D turbulence in thin electrolyte solutions in a rectangular container [16, 17]. These investigators claim correspondence between their results and the theory proposed by Carnevale and coworkers.

In several studies it has been observed recently that vorticity produced near no-slip walls modifies the decay process of 2D turbulence considerably [19–21]. The source of vorticity is found in the thin boundary layers at the no-slip walls, and after boundary layer detachment these filaments are either advected into the interior of the flow domain or they roll up and form new vortices. One of the tools to understand the role of the boundaries in the evolution of turbulence is by comparing the energy spectra computed for simulations with no-slip and with periodic boundary conditions. It is obvious that isotropy and homogeneity are absent when no-slip walls confine the flow. As a consequence an alternative approach has to be used to measure the energy spectra for the no-slip and the periodic case. For this purpose, a 1D spectrum is used based on the 2D Chebyshev expansion of the (dimensionless) kinetic energy of the flow

$$E(x, y, \tau) = \sum_{n=0}^{N} \sum_{m=0}^{N} \hat{E}_{nm}(\tau) T_n(x) T_m(y), \tag{1}$$

along a line parallel to one of the boundaries. The $T_n(x)$ and $T_m(y)$ are the Chebyshev polynomials, and the $\hat{E}_{nm}(\tau)$ represent the (time-dependent) Chebyshev spectral coefficients of the kinetic energy. The 1D spectrum $\hat{S}_n(\tau)$ is defined as an average of the symmetrically equivalent contributions along the lines $x = a$, $x = -a$, $y = a$, and $y = -a$ which are all parallel to one of the boundaries. The 1D spectrum of the contribution along

the line $x = a$, denoted by $\hat{S}_{x=a,n}(\tau)$, is expressed as

$$\hat{S}_{x=a,n}(\tau) = \left| \sum_{m=0}^{N} \hat{E}_{mn}(\tau) T_m(a) \right|_{\Delta\tau}, \tag{2}$$

where the subscript $\Delta\tau$ states that the 1D spectrum is averaged over the time interval $[\tau - \Delta\tau, \tau]$ with $\Delta\tau$ of the order of the initial eddy turnover time. The 1D spectra for the simulations with periodic boundary conditions are computed in a similar way. An interesting observation is the following: the inertial range of the 1D energy spectrum, measured along a line parallel with one of the boundaries not too far from this boundary, shows a $k^{-5/3}$-slope up to the smallest wave numbers used in the simulations (length scales as small as the enstrophy dissipation scale are well resolved). The presence of the $k^{-5/3}$-slope for small wave numbers is due to the production of small-scale vorticity filaments near the no-slip walls [20]. The direct enstrophy cascade is virtually absent at early times during the decay process. To illustrate this remarkable feature we have plotted in *figure 1* the averaged 1D energy spectrum for runs with freely evolving 2D turbulence, with $Re = 20{,}000$, in double periodic domains and for similar runs in domains with no-slip boundaries. The average spectrum computed for the runs with periodic boundary conditions shows reasonable agreement with the predicted $k^{-3}$-slope for large wave numbers. This spectrum is measured after approximately four initial eddy turnover times ($\tau = 4$). The 1D energy spectrum for the no-slip runs, measured near the boundaries, shows at the same time a $k^{-5/3}$-slope instead of a $k^{-3}$-slope (*figure 1(b)*). When the spectra are measured at a larger distance from the boundary, the clear $k^{-5/3}$-slope slowly disappears but the spectra for runs with periodic and with no-slip boundary conditions remain different (see for more details [20]). At later times the energy spectrum shows the build-up of a direct enstrophy cascade with a $k^{-3}$ inertial range together with the inverse energy cascade for smaller wave numbers (see *figure 1(c)*). The energy spectrum shows a kink, which slowly moves to smaller wave numbers. The position of the kink, which represents the injection scale $k_i$, can clearly be associated with the growth of an averaged local boundary-layer thickness. The spectra as observed in these simulations differ

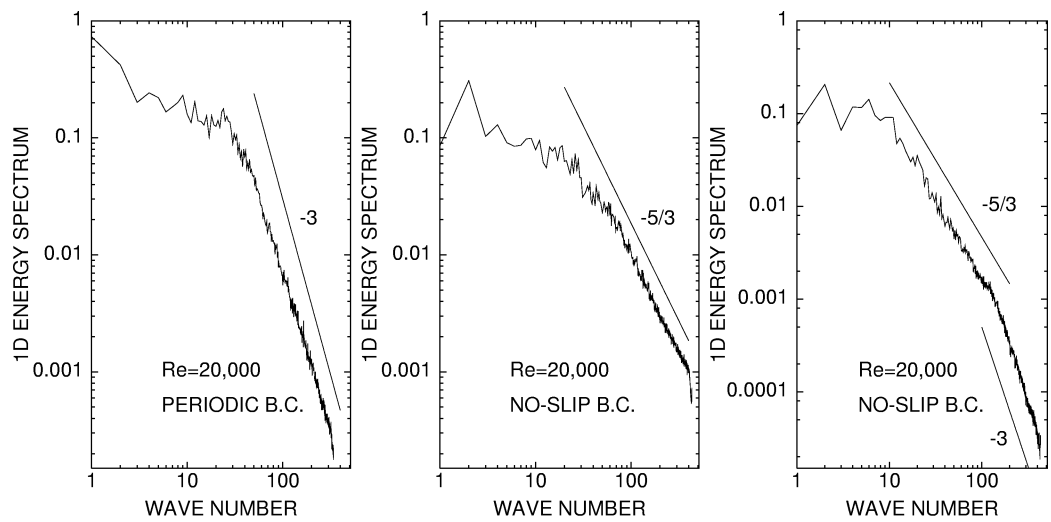


(a) $\tau = 4$ (b) $\tau = 4$ (c) $\tau = 32$

**Figure 1.** Averaged 1D energy spectra for runs with $Re = 20{,}000$.

**Table I.** Power-law exponents for runs with no-slip and with periodic boundary conditions for $Re = 5{,}000$ and 10,000. The last row represents the exponents as obtained form the theory by Carnevale and coworkers with $\zeta = 0.72$.

| $Re$ | $\langle \frac{\omega_{ext}}{\sqrt{E}} \rangle_{no\text{-}slip}$ | $\langle Z/E \rangle_{no\text{-}slip}$ | $\langle \rho \rangle_{no\text{-}slip}$ | $\langle r \rangle_{no\text{-}slip}$ | $\langle a \rangle_{no\text{-}slip}$ |
|---|---|---|---|---|---|
| 5,000 | $-0.35 \pm 0.05$ | $-0.80 \pm 0.1$ | $-0.85 \pm 0.1$ | $0.45 \pm 0.07$ | $0.25 \pm 0.03$ |
| 10,000 | $-0.30 \pm 0.05$ | $-0.70 \pm 0.1$ | $-0.75 \pm 0.1$ | $0.40 \pm 0.07$ | $0.25 \pm 0.03$ |
| $Re$ | $\langle \frac{\omega_{ext}}{\sqrt{E}} \rangle_{periodic}$ | $\langle Z/E \rangle_{periodic}$ | $\langle \rho \rangle_{periodic}$ | $\langle r \rangle_{periodic}$ | $\langle a \rangle_{periodic}$ |
| 5,000 | $-0.47 \pm 0.04$ | $-1.13 \pm 0.05$ | $-1.13 \pm 0.1$ | $0.65 \pm 0.05$ | $0.25 \pm 0.03$ |
| 10,000 | $-0.38 \pm 0.04$ | $-0.98 \pm 0.05$ | $-1.03 \pm 0.1$ | $0.60 \pm 0.05$ | $0.25 \pm 0.03$ |
| | $\frac{\omega_{ext}}{\sqrt{E}}$ | $Z/E$ | $\rho$ | $r$ | $a$ |
| | 0 | –0.36 | –0.72 | 0.36 | 0.18 |

from the well-known Kraichnan–Batchelor picture of 2D turbulence mentioned earlier, and differ also with spectra computed from our simulations with periodic boundary conditions.

Actually, the boundaries act as generators of vortices, thus modifying the evolution of vortex statistics. Numerical studies of decaying 2D Navier–Stokes turbulence in containers with no-slip boundaries show a distinctly different evolution of vortex statistics, at least up to integral-scale Reynolds numbers of 20,000, than predicted on basis of the theory proposed by Carnevale et al. [14,15]. The evolution of vortex statistics of freely evolving 2D turbulence in square domains with no-slip boundaries is also compared with similar numerical experiments with periodic boundary conditions, and the differences between the two approaches are striking. In *table I* we have summarised the power-law exponents computed for runs with periodic and with no-slip boundary conditions, with $\omega_{ext}/\sqrt{E}$, $Z/E$, $\rho$, $r$, and $a$ the normalised vorticity extremum, the normalised enstrophy, the vortex density, the mean vortex separation and the vortex radius, respectively, and $\langle \cdot \rangle$ denotes an ensemble average over approximately 10 runs (see for more details [21]). It is still an open question whether the observed difference in the evolution of vortex statistics for decaying 2D turbulence depends indeed on the type of boundary conditions. Higher Reynolds number simulations are necessary to investigate the sensitivity to particular boundary conditions. An additional complication, which has not been discussed here, is the role of the initial flow field on vortex statistics.

We have also computed the power-law exponents for the final decay stage where viscous effects are relatively important [21], and these data show agreement with the measured values by Hansen et al. [17] in experiments with relatively small initial integral-scale Reynolds number of the flow ($Re \approx 1{,}000$). Therefore we have the impression that any agreement between the power-law exponents obtained in these experiments and the power-law exponents from the theory by Carnevale and coworkers is rather accidental; the results seem to coincide better with our final decay stage data.

Another interesting observation from numerical simulations of decaying 2D turbulence in square domains with no-slip walls is the spontaneous spin-up of the flow due to shear and normal forces exerted by the walls on the fluid in the container [19]. In the first part of this paper we discuss this issue in more detail with numerical data from high Reynolds number decaying turbulence simulations with different initialisation procedures. Before proceeding to this issue we give an outline of the numerical method and introduce the two initialisation procedures used in present spin-up study.

## 3. Initialisation procedure

The numerical simulations of the 2D Navier–Stokes equations on a bounded domain with no-slip walls were performed with a 2D de-aliased Chebyshev pseudospectral method [22]. The flow domain $D$ with boundary

$\partial D$ is a two-dimensional square cavity. Cartesian coordinates are denoted by $x$ and $y$, and the velocity field is denoted by $\mathbf{u} = (u, v)$. The equation governing the (scalar) vorticity $\omega = \frac{\partial v}{\partial x} - \frac{\partial u}{\partial y}$ is obtained by taking the curl of the momentum equation. The following set of equations has been solved numerically:

$$\frac{\partial \omega}{\partial t} + (\mathbf{u} \cdot \nabla)\omega = \nu \nabla^2 \omega, \tag{3}$$

$$\nabla^2 \mathbf{u} = \mathbf{k} \times \nabla \omega, \tag{4}$$

with the boundary condition $\mathbf{u} = \mathbf{0}$ and enforcing $\mathbf{k} \cdot \nabla \times \mathbf{u} = \omega$ on $\partial D$ by an influence matrix method [22]. An initial condition, $\omega|_{t=0} = \mathbf{k} \cdot \nabla \times \mathbf{u}_i$, where $\mathbf{u}_i$ is the initial velocity field, is also supplemented. In present numerical simulations of the Navier–Stokes equations neither hyperviscosity nor any other artificial dissipation has been used. The time discretisation of the vorticity equation is semi-implicit: it uses the explicit Adams–Bashforth scheme for the advection term and the implicit Crank–Nicolson procedure for the diffusive term. Both components of the velocity and the vorticity are expanded in a double truncated series of Chebyshev polynomials. All numerical calculations, except the evaluation of the nonlinear terms, are performed in spectral space, i.e. the Chebyshev coefficients are marched in time. Fast Fourier Transform methods are used to evaluate the nonlinear terms following the procedure designed by Orszag [23], where the padding technique has been used for de-aliasing.

The integral-scale Reynolds number of the flow is defined as $Re = UW/\nu$ with $U$ the RMS velocity of the initial flow field, $W$ the half-width of the container and $\nu$ the kinematic viscosity of the fluid. Time has been made dimensionless by $W/U$ and vorticity by $U/W$. The initial micro-scale Reynolds number is defined as: $Re_{micr} = 2Re/\omega_0$ [24], with $\omega_0$ the (dimensionless) initial RMS vorticity.

Two kinds of numerical experiments have been performed: a set of numerical simulations with a random initial velocity field and relatively small integral-scale Reynolds numbers ($1{,}000 \leqslant Re \leqslant 2{,}000$), and another set with $10 \times 10$ slightly perturbed Gaussian vortices on a regular lattice. The integral-scale Reynolds number for this latter set of simulations is considerably higher: $5{,}000 \leqslant Re \leqslant 20{,}000$. Both initialisation procedures are briefly described.

For the first kind of numerical experiments the initial condition for the velocity field, denoted by $\mathbf{u}_i$, is obtained by a zero-mean Gaussian random realisation of the first $65 \times 65$ Chebyshev spectral coefficients of both $u_i$ and $v_i$, and subsequently applying a smoothing procedure in order to enforce $\mathbf{u}_i = \mathbf{0}$ at the boundary of the domain. The variance $\sigma_{nm}$ of the velocity spectrum of $\mathbf{u}_i$ is chosen as

$$\sigma_{nm}^2 = \frac{n}{[1 + (\frac{1}{8}n)^4]} \frac{m}{[1 + (\frac{1}{8}m)^4]}, \tag{5}$$

with $0 \leqslant n, m \leqslant 64$, and $\sigma_{nm} \equiv 0$ for $n, m \geqslant 65$, and the resulting flow field is denoted by $\mathbf{U}(x, y)$. The smoothing function is chosen as $f(x) = [1 - \exp(-\beta(1 - x^2)^2)]$, with $\beta = 100$. The initial velocity field is thus: $\mathbf{u}_i(x, y) = f(x) f(y) \mathbf{U}(x, y)$, where the flow field is normalised in order to enforce the $L^2$-norm of the velocity per unit surface of the initial flow field to be equal to unity. The minimum number of Chebyshev modes required to get a well-resolved simulation of the flow dynamics for this particular kind of computations scales like $N \simeq 6\sqrt{Re}$ [25]. We have used $N = 180$, 256 and 288 for $Re = 1{,}000$, 1,500 and 2,000, respectively, all satisfying the well-resolvedness condition. In these numerical experiments we find for the dimensionless initial RMS vorticity $\omega_0 = 28.0 \pm 0.5$, thus $Re_{micr} \cong 71$, 107 and 143, respectively.

The initial condition for the velocity field in the second set of numerical experiments consists of 100 nearly equal-sized Gaussian vortices. The vortices have a dimensionless radius of 0.05 and a dimensionless

absolute vortex amplitude of $|\omega_{\max}| \cong 100$. Half of the vortices have positive circulation, and the other vortices have negative circulation. The vortices are placed on a regular lattice, well away from the boundaries, with a random displacement of the vortex centres equal to approximately 6% of the dimensionless lattice parameter $\lambda$, with $\lambda \cong 0.17$. A smoothing function, similar to the one employed in the previous initialisation procedure, has been used in order to ensure the no-slip condition exactly. The initial micro-scale Reynolds number for these simulations is substantially higher then for the previous set: $Re_{micr} \cong 263, 526$ and 1052, respectively ($\omega_0 = 38.0 \pm 0.5$). These computations are more demanding and require a relatively large number of Chebyshev modes for the simulations. The number of modes depends on the local enstrophy dissipation scale $\lambda_d \cong 2\pi(\nu^3/\varepsilon)^{1/6}$, with $\varepsilon$ the instantaneous enstrophy decay rate per unit area. The local enstrophy dissipation scale has to be resolved reasonably well in the domain and near the boundaries. The number of modes is now 257, 361 and 513 for $Re = 5{,}000$, 10,000 and 20,000, respectively. For this set of initial conditions we can introduce a new dimensionless time $\tau$, defined as $\tau = \frac{1}{10}\omega_0 t$ (with $t$ the dimensionless time based on the characteristic parameters $W$ and $U$), and $\tau = 1$ corresponds approximately with the initial eddy turnover time of the Gaussian vortices. We will employ the same definition of $\tau$ for the simulations with random initial vorticity fields, because it appeared that the number of coherent structures which arise from the random flow field is, by accident, approximately 100 (see [25], figure 5c). Note, however, that we have to use the slightly smaller value for the RMS vorticity in that case: $\omega_0 = 28.0$.

The kinetic energy $E(t)$, the enstrophy $\Omega(t)$ and the palinstrophy $P(t)$ of the flow are defined as

$$E(t) = \frac{1}{2}\int_D \mathbf{u}^2(\mathbf{r}, t)\,\mathrm{d}A, \tag{6}$$

$$\Omega(t) = \frac{1}{2}\int_D \omega^2(\mathbf{r}, t)\,\mathrm{d}A, \tag{7}$$

$$P(t) = \frac{1}{2}\int_D \left(\nabla\omega(\mathbf{r}, t)\right)^2\,\mathrm{d}A, \tag{8}$$

with $D$ denoting the domain and $\mathrm{d}A$ an infinitesimal surface element of $D$. The meaning of the energy and the enstrophy is straightforward. The palinstrophy, however, is less often used. It is a global average of the vorticity gradients in the flow. For decaying high Reynolds number 2D turbulence in double periodic domains vortex mergings can be recognised by inspection of the palinstrophy: each merging is represented by a strong peak in the palinstrophy evolution. When no-slip boundaries are present the time evolution of the palinstrophy is completely dominated by vortex-wall interactions. For a bounded domain with no-slip walls the time rate of change of the energy is exactly the same as found for flows in domains with periodic boundary conditions: $\frac{\mathrm{d}E(t)}{\mathrm{d}t} = -2\nu\Omega(t)$. The time rate of change of the enstrophy contains an additional term which is related with the vorticity as well as the vorticity gradients at the no-slip boundary (see also [26] for flows in an annular geometry),

$$\frac{\mathrm{d}\Omega(t)}{\mathrm{d}t} = -2\nu P(t) + \nu\oint_{\partial D}\omega(\mathbf{r}, t)\frac{\partial\omega(\mathbf{r}, t)}{\partial n}\,\mathrm{d}s, \tag{9}$$

with $\partial/\partial n$ denoting the normal derivative with respect to the boundary $\partial D$ and $\mathrm{d}s$ the length of an infinitesimal element of the boundary $\partial D$. The ensemble-averaged energy, enstrophy and palinstrophy for numerical experiments (with $Re = 10{,}000$ and where the average is based on eight different runs) with periodic and with no-slip boundaries have been plotted in *figures 2(a)–(c)*. The ensemble-averaged values of $E(t)$, $\Omega(t)$ and $P(t)$ are computed up to $\tau = 200$ for the periodic runs and up to $\tau = 500$ for the no-slip runs. Enhanced dissipation of kinetic energy of the flow in the simulations with no-slip boundaries is clearly visible in *figure 2(a)*. The

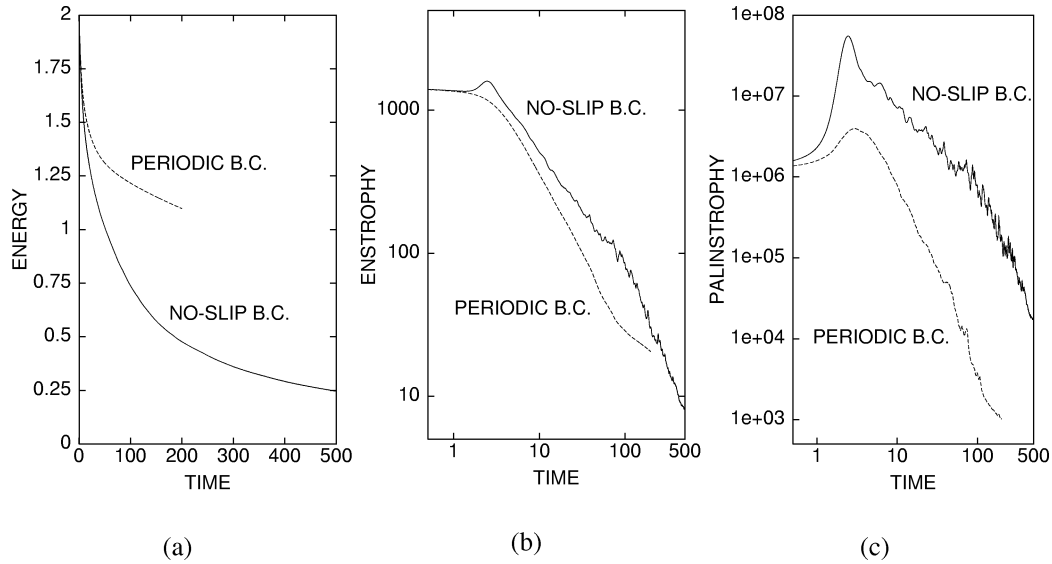


**Figure 2.** The averaged (a) kinetic energy $E(\tau)$, (b) enstrophy $\Omega(\tau)$ and (c) palinstrophy $P(\tau)$ for runs with periodic boundaries (dotted lines) and no-slip boundaries (drawn lines). The initial integral-scale Reynolds number is 10,000.

effective Reynolds number $Re(\tau)$, based on the kinetic energy $E(\tau)$, has decreased at $\tau = 200$ to approximately 5,000 for the no-slip runs and 7,500 for the runs with periodic boundary conditions. The decrease of the enstrophy (*figure 2(b)*) indicates that self-organisation of the flow, and the associated appearance of large scale vortices (note that the average size of the vortices can be inferred from $\sqrt{E(\tau)/\Omega(\tau)}$), occurs more rapidly for freely evolving 2D turbulence with periodic boundaries compared to the no-slip case (as might be expected because no-slip walls serve as a source of small-scale vorticity). The role of no-slip walls on the palinstrophy evolution is illustrated in *figure 2(c)*: the production of vorticity gradients is substantially larger, and the subsequent decay of the palinstrophy is slower than for runs with periodic boundary conditions (the palinstropy is one to two orders of magnitude smaller in the periodic case). Vortex-wall interactions are represented by the spikes in the palinstrophy plot for the no-slip case. Note that these plots represent ensemble averages, thus most of the spiky behaviour has been suppressed by the averageing procedure.

## 4. Spontaneous spin-up during the decay of turbulence

The flow evolution of decaying 2D turbulence on a square domain with no-slip walls is characterised by three stages. Rapid self-organisation due to merging of like-sign vortices and the formation of medium-sized dipoles are the main features of the initial stage. Actually, this stage is the vigorous turbulent decay phase. The second stage is characterised by the presence of strong vortex-wall interactions and the formation of increasingly larger coherent structures. In the third stage a relaxation process to a tripolar or monopolar structure is observed. This structure, with a size comparable with the container dimension, is more or less situated in the centre of the container. During the final stage, when most of the initial kinetic energy of the flow is dissipated, the flow is dominated by viscous relaxation. This part of the decay process will not be discussed. During the initial and intermediate decay stage a remarkable process is observed for the large majority of the runs: the (absolute value of the) angular momentum of the flow, which was initially approximately zero, increases dramatically. This sudden increase of the angular momentum reflects the ‘spontaneous spin-up’ of the flow. Since the angular momentum of unbounded viscous flows is conserved when the total circulation is zero, spontaneous spin-up is

a process which is entirely due to the finiteness of the flow. This is easily understood by considering the angular momentum $L(t)$, defined with respect to the centre of the container,

$$L(t) = \int_D \left[ x v(\mathbf{r}, t) - y u(\mathbf{r}, t) \right] \mathrm{d}A = -\frac{1}{2} \int_D r^2 \omega(\mathbf{r}, t)\, \mathrm{d}A, \tag{10}$$

and its time derivative. The expression of $L(t)$ in terms of the vorticity is obtained by partial integration and using the boundary condition for the velocity. It is clear from equation (10) that two versions of $\mathrm{d}L(t)/\mathrm{d}t$ can be derived which are equivalent: one based on the Navier–Stokes equations,

$$\frac{\mathrm{d}L(t)}{\mathrm{d}t} = \frac{1}{\rho} \oint_{\partial D} p(\mathbf{r}, t)\mathbf{r} \cdot \mathrm{d}\mathbf{s} + \nu \oint_{\partial D} \omega(\mathbf{r}, t)(\mathbf{r} \cdot \mathbf{n})\, \mathrm{d}s, \tag{11}$$

and one derived from the vorticity equation (3),

$$\frac{\mathrm{d}L(t)}{\mathrm{d}t} = -\frac{1}{2}\nu \oint_{\partial D} r^2 \frac{\partial \omega}{\partial n}\, \mathrm{d}s + \nu \oint_{\partial D} \omega(\mathbf{r}, t)(\mathbf{r} \cdot \mathbf{n})\, \mathrm{d}s, \tag{12}$$

with $\mathbf{n}$ the unit vector normal to the boundary, $\partial/\partial n$ denoting the normal derivative with respect to the boundary $\partial D$ and $\mathrm{d}\mathbf{s}$ an infinitesimal tangential element of the boundary $\partial D$. The last contribution to equation (11) and (12) is simplified in case of a square domain: $\nu W \oint_{\partial D} \omega(\mathbf{r}, t)\, \mathrm{d}s$, and it represents the stress on the no-slip boundary. In the derivation of equations (11) and (12) we have used that the total circulation for flows in bounded domains with stationary no-slip walls is zero. We like to mention both formulations of $\mathrm{d}L(t)/\mathrm{d}t$ because it clarifies the role of several physical processes determining the time-dependence of the angular momentum. From both relations we conclude that the total shear stress along the boundary influences the time rate of change of $L(t)$. Additionally, a pressure contribution will also modify the time rate of change of $L(t)$. It is clear from equation (12) that this contribution should be proportional to the normal vorticity gradient integrated over the boundary.[2] It is interesting to note that the product $\nu \frac{\partial \omega}{\partial n}$ should be finite for vanishing viscosity (thereby assuming a finite pressure contribution in the expression for $\mathrm{d}L(t)/\mathrm{d}t$ in this limiting case).

Spontaneous spin-up of decaying 2D turbulence with a random initial velocity field is clearly observed for $Re = 1{,}500$ and 2,000. For $Re = 1{,}000$ viscous effects are relatively strong, and the spin-up process occurs less frequently. Four examples of spin-up are shown in *figure 3*: two examples from decaying 2D turbulence with random initial vorticity field (*figure 3(a)*) and two examples obtained from runs with initially 100 Gaussian vortices on a regular lattice (*figure 3(b)*). We first discuss briefly spontaneous spin-up from random initial velocity fields. The absolute value of the (dimensionless) angular momentum of the flow in one of these runs (see upper curve in *figure 3(a)*) increases suddenly from the dimensionless value $|L| \cong 0$ to $|L| \cong 0.3$ during a short time interval ($15 \leqslant \tau \leqslant 50$), and decays afterwards very slowly ($|L| \cong 0.15$ for $\tau = 300$). Inspection of the vorticity contour plots of this simulation shows, as is the case for all runs with similar initial conditions and which show spontaneous spin-up, that the maximum absolute angular momentum is associated with the appearance of one relatively strong vortex somewhere in the centre of the container: the spin-up process is dominated by the formation and dynamics of one vortex. In this set of simulations it appears that approximately 65% of the runs show spontaneous spin-up; 20% of the runs show weak spin-up (i.e. at early times spin-up is observed but a relatively rapid decay of the dominant vortex results in fast decay of $|L|$) and 15% of the runs

[2] Equivalence of both terms can also be shown by expressing the pressure boundary condition for present problem in terms of the normal vorticity gradient at the boundary.

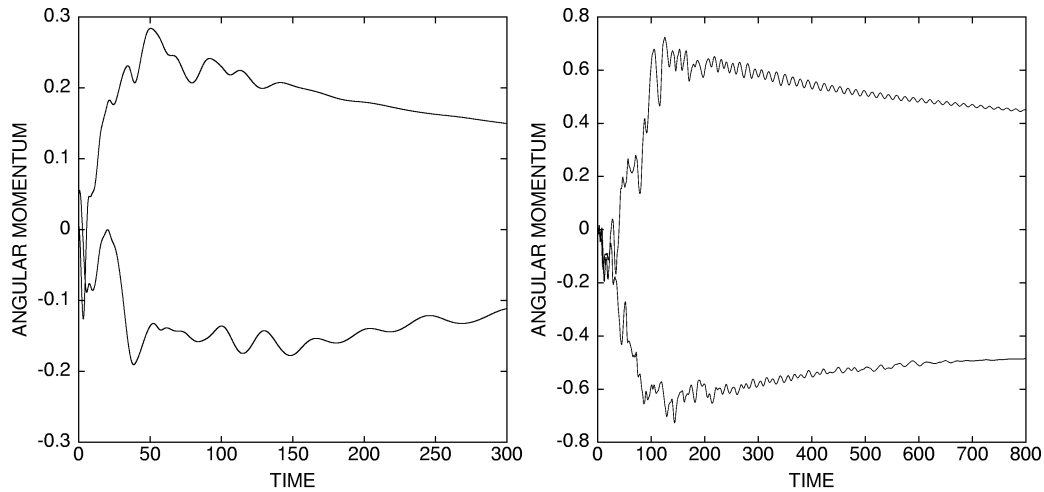


**Figure 3.** The dimensionless angular momentum for four numerical simulations in square containers with no-slip walls. In (a) the flow is initialised with a random initial vorticity field ($Re = 2{,}000$) and in (b) with an array of $10 \times 10$ Gaussian vortices ($Re = 10{,}000$).

**Table II.** We have summarised for each integral-scale Reynolds number the total number of runs $N$, the number of runs showing spontaneous spin-up ($N_s$) and weak spin-up ($N_w$), the characteristic spin-up times $T_{spin\text{-}up}$ and amplitudes $A_{spin\text{-}up}$. The error in $T_{spin\text{-}up}$ is approximately 40%, and the error in $A_{spin\text{-}up}$ is roughly 15%.

| $Re$ | $N$ | $N_s$ | $N_w$ | $T_{spin\text{-}up}$ | $A_{spin\text{-}up}$ |
|---|---|---|---|---|---|
| 1,000 | 12 | 7 | 1 | 36 | 0.14 |
| 1,500 | 12 | 8 | 2 | 60 | 0.20 |
| 2,000 | 13 | 8 | 3 | 51 | 0.22 |
| 5,000 | 12 | 8 | 3 | 148 | 0.44 |
| 10,000 | 8 | 8 | 0 | 149 | 0.67 |
| 20,000 | 2 | 2 | 0 | 136 | 0.56 |

show no spin-up at all. Several characteristics from an ensemble of simulations with random initial velocity field are summarised in *table II*. The characteristic spin-up amplitude $A_{spin\text{-}up}$ summarised in *table II* is based on the average value of the maximum of $|L(t)|$ of the runs showing spontaneous spin-up. The average time necessary for spin-up of the flow is denoted by the characteristic spin-up time $T_{spin\text{-}up}$ (only data from runs showing spontaneous spin-up are used for the ensemble average).

The spontaneous spin-up phenomenon is even more pronounced when the Reynolds number is increased with an order of magnitude. We illustrate this with a few simulations where the initial vorticity field consists of a checker board pattern of Gaussian vortices with alternating sign. The initial angular momentum is approximately zero (as is the case for all our runs) and $Re = 10{,}000$. In *figure 3(b)* we have plotted the dimensionless angular momentum for two runs and the spin-up of the flow is rather obvious in both cases. The upper curve shows $L(t)$ of a run (displayed in *figure 4*) which we discuss in more detail. Although $L(t = 0) \cong 0$ it rapidly grows to $L = 0.73$ at $\tau \cong 120$. After reaching a maximum, the dimensionless angular momentum slowly decreases to $L \cong 0.45$ at $\tau = 800$. The oscillation of the angular momentum reflects the presence of a rapidly rotating tripolar structure located in the centre of the container. The local minima in the graph of $L(t)$ correspond to the situation where the satellite vortices are located in the two diagonally opposite corners of the

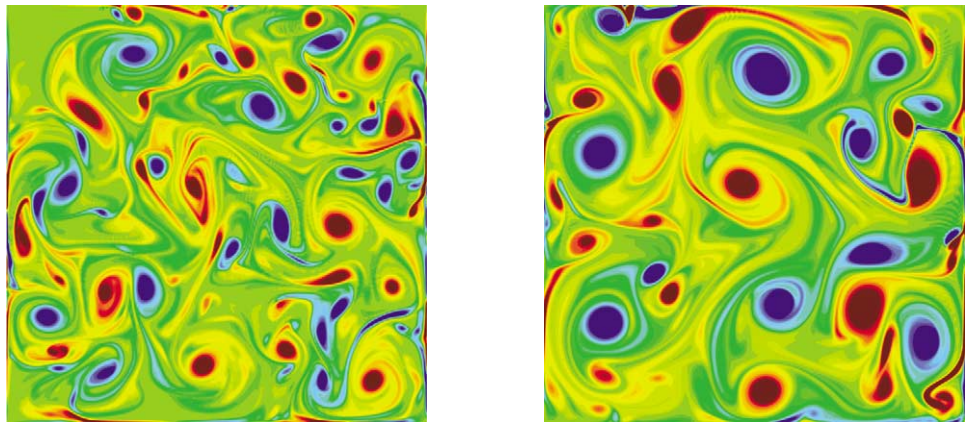

(a) $\tau = 8$ (b) $\tau = 20$

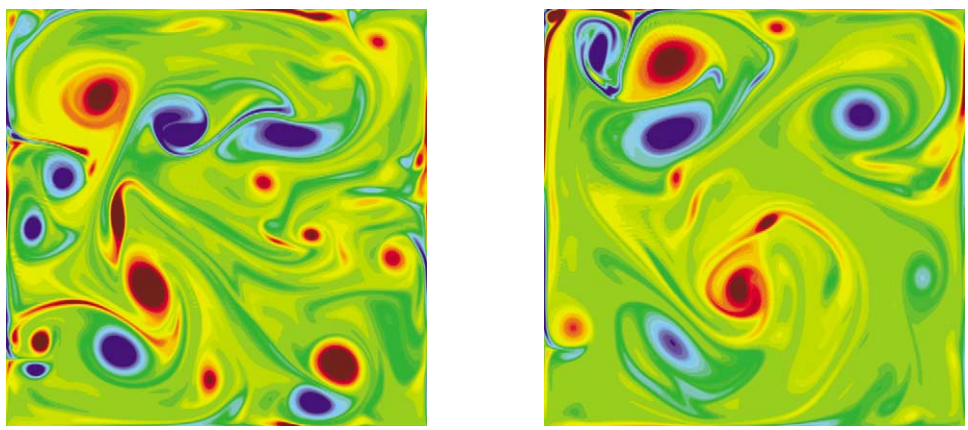

(c) $\tau = 40$ (d) $\tau = 80$

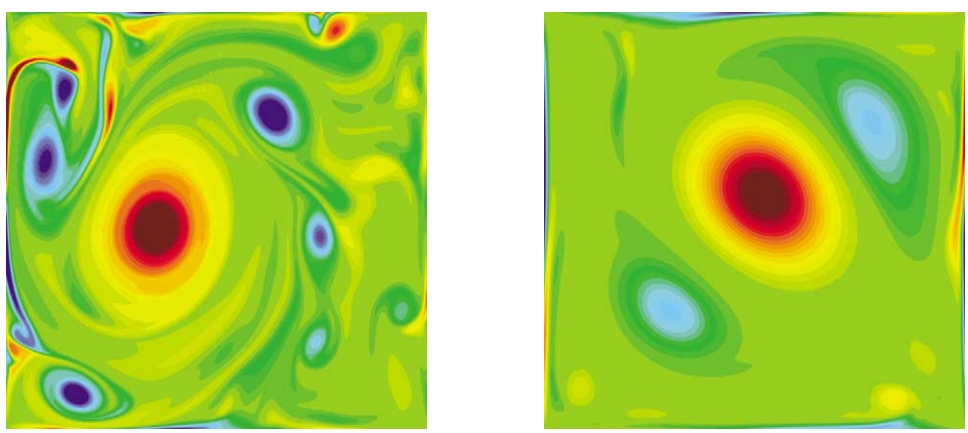

(e) $\tau = 200$ (f) $\tau = 400$

**Figure 4.** Vorticity plots of a simulation with no-slip boundary conditions ($Re = 10{,}000$). Red indicates positive vorticity, blue indicates negative vorticity and $\tau = 1$ corresponds to one initial eddy turnover time.

domain. The angular momentum shows a local maximum when the axis of the tripole, i.e. the (approximately straight) line joining the two satellites with the central vortex, is parallel with two of the boundaries. In principle, the time rate of chance of $L(t)$ can be explained by interpreting the contributions in equations (11) and (12). A comparison between these two contributions reveals that $\mathrm{d}L(t)/\mathrm{d}t$ is dominated by the normal vorticity gradient integrated over the boundary (or by the pressure distribution integrated over the boundary) and is thus hardly influenced by the total shear stress along the boundary. This striking difference between the relative importance of both terms determining $\mathrm{d}L(t)/\mathrm{d}t$ appears more generally valid for our decaying turbulence simulations. A few snapshots of the vorticity field of this particular run are shown in *figure 4*. The production of vorticity near the no-slip boundaries is clearly visible in all snapshots and in *figures 4(a)–(e)* one can also observe detachment of boundary layers which subsequently roll up and form small-scale vortices. Evidence of the presence of a large tripole is nicely illustrated in *figure 4(f)*. A rather important difference between the decay process of turbulence, and the spin-up phenomenon in particular, for the two sets of simulations is the following: the complete process of spontaneous spin-up observed in the intermediate Reynolds number case ($1{,}000 \leqslant Re \leqslant 2{,}000$) coincides with the formation of a tripolar or a monopolar vortex with characteristic size comparable with the container dimension. In the high Reynolds number case it is observed that during the spin-up stage of freely evolving 2D turbulence the average scale of the vortices is still rather small: spontaneous spin-up of the flow is reflected by the build-up of mean background rotation of the flow. As a result the sea of vortices is rotating with respect to the container boundaries. This can be seen in, e.g. *figure 4(e)* ($\tau = 200$) where small-scale vortices with negative circulation (the blue patches) are moving around a somewhat larger positive vortex (note that the maximum of $L(t)$ occurred already for $\tau \approx 100$). It is remarkable that, in contrast to the runs with lower Reynolds number, all runs with $Re = 10{,}000$ show spontaneous spin-up (see *table II* where also $T_{spin\text{-}up}$ and $A_{spin\text{-}up}$ for these runs are summarised) and that only one run out of twelve with $Re = 5{,}000$ show no spin-up at all. The two runs with $Re = 20{,}000$ show spontaneous spin-up, but the total number of runs is too small in this case to be statistically significant. Furthermore, the averaged values for $T_{spin\text{-}up}$ and $A_{spin\text{-}up}$ computed from these runs are most likely lower bounds due to limitation in computation time ($\tau \leqslant 200$) for these simulations (several hundred CPU hours per run on a Cray Y-MP C916). Nevertheless, we expect from the limited data available for this set of runs that once more nearly all runs show spontaneous spin-up.

It is worthwhile to note that the final states obtained in runs showing spontaneous spin-up have a partially relevant analogon for 2D bounded Euler flows.[3] For the case of 2D Euler flows a framework exists in which such behaviour might be expected as is shown by Pointin and Lundgren in a calculation of most probable, or maximum-entropy, states in a square container [27] (see also [28,29]). In their calculations they showed on statistical mechanical grounds a most-probable state for that situation as one containing a large central vortex core of one sign, surrounded by a vorticity distribution of opposite sign for the zero net vorticity case. Such a configuration necessarily has a large angular momentum, even if it developed from a state with none. No such general framework exists for the bounded case with no-slip walls where viscosity cannot be disregarded.

## 5. Forced 2D turbulence

Recently, numerical studies revealed the special role of the angular momentum in decaying 2D turbulence in circular containers with no-slip walls by Li and Montgomery [30], and experimental confirmation of several of their findings has been presented by Maassen et al. [31]. Both the simulations and the experiments are carried out at relatively low Reynolds numbers. Here we will report on an investigation of an alternative case: forced 2D

[3] Note, however, that spontaneous spin-up for decaying 2D turbulence with high initial integral-scale Reynolds number is characterised by many small-scale structures in a large-scale background flow with mean rotation.

turbulence in a circular domain with no-slip boundary conditions. The integral-scale Reynolds number in these numerical experiments, reached after a certain time of forcing, are considerably larger than in the simulations and experiments on decaying 2D turbulence mentioned above.

In this section we compare the flow dynamics of forced 2D turbulence in a circular domain with a no-slip wall to the flow evolution in an unbounded domain. For this purpose the 2D incompressible Navier–Stokes equations are written in the vorticity-stream function formulation:

$$\frac{\partial \omega}{\partial t} + J(\omega, \psi) = \nu \nabla^2 \omega + F, \tag{13}$$

with $\nu$ the kinematic viscosity and $F$ a forcing term which will be described below. For completeness we recall that $\omega$ is the scalar vorticity and $\psi$ is the stream function which is related to the vorticity by the Poisson equation

$$\nabla^2 \psi = -\omega. \tag{14}$$

The Jacobian $J(\omega, \psi)$ is given by

$$J(\omega, \psi) = \frac{\partial \omega}{\partial x}\frac{\partial \psi}{\partial y} - \frac{\partial \psi}{\partial x}\frac{\partial \omega}{\partial y} = \frac{1}{r}\left[\frac{\partial \omega}{\partial r}\frac{\partial \psi}{\partial \theta} - \frac{\partial \psi}{\partial r}\frac{\partial \omega}{\partial \theta}\right]. \tag{15}$$

We use two different pseudospectral algorithms to solve equations (13) and (14). For the unbounded domain we use a standard 2D Fourier pseudospectral method. Hereby we obtain a double periodic domain, and the length of each cell is set to $L_x = L_y = L = 2.0$. We note that even though we are only regarding simulations in a finite square box, a double periodic domain is in principal an infinite domain with the (artificial) restriction that a subsection of the domain is repeated indefinitely.

For the circular domain we use a disk code which solves equations (13) and (14) on a circular domain with radius $R = 1$. The solutions for $\omega$ and $\psi$ are expanded into series of Chebyshev polynomials for the radial direction and Fourier modes in the azimuthal direction. The Chebyshev polynomials are here defined on the entire interval $-R \leqslant r \leqslant R$ in order to avoid having a large concentration of points near the origin. As boundary condition we use the no-slip condition, i.e. $u_r(R, \theta, t) = 0$ and $u_\theta(R, \theta, t) = 0$. A description of the disk code can be found in [32].

For both codes we are using an implicit 3rd order stiffly-stable time integration scheme. The resolution of the simulations with periodic boundary conditions is $N = M = 256$ in all the simulations whereas for the computations in a circular domain with a no-slip wall we used $N = M = 512$. For both codes we have used low level noise as initial condition. The definition of the integral-scale Reynolds number for the simulations with periodic boundary conditions is the same as the one employed previously for the computations of decaying 2D turbulence in square domains with no-slip boundaries: $Re = \frac{1}{2}L\sqrt{\langle \mathbf{u}^2 \rangle}/\nu = \sqrt{\frac{1}{2}E(t)}/\nu$ with the kinetic energy $E(t)$ defined as in equation (6). In case of the circular domain the integral-scale Reynolds number is defined as $Re = R\sqrt{\langle \mathbf{u}^2 \rangle}/\nu = \sqrt{\frac{2}{\pi}E(t)}/\nu$ (in this case $D$ in equation (6) represents the circular domain).

The forcing term which we employ in present numerical study is constructed to be both homogeneous and isotropic. In addition we attempt to make the forcing term as identical as possible for the two different domains. To achieve this we first consider the unbounded domain in Fourier space and we activate certain modes of this system,

$$F(x, y, t) = c \sum_{k_x=-N/2}^{N/2-1} \sum_{k_y=-M/2}^{M/2-1} G(|\mathbf{k}|) \exp\left(\frac{2\pi i k_x x}{L}\right) \exp\left(\frac{2\pi i k_y y}{L}\right) \exp\big(i\Theta(t)\big), \tag{16}$$

where $c$ is a constant and $\Theta(t)$ is a phase which is diffusing randomly in time with a diffusion time scale $\tau_{diff}$. We have performed simulations with the diffusion time scale ranging from $\tau_{diff} = 0.01$ (corresponding to nearly completely random forcing in time) to $\tau_{diff} = 100$ (corresponding to nearly static forcing). Qualitatively we find no significant differences using the different values of $\tau_{diff}$. In this section we will show the results for $\tau_{diff} = 0.1$ in order to display the differences observed in the two domains (bounded versus periodic). Furthermore, for the bounded case we also present the results for $\tau_{diff} = 100$.

The filter function, $G$, is defined by

$$G(|\,\mathbf{k}\,|) = \begin{cases} 1 & \text{if } a < |\mathbf{k}| < b, \\ 0 & \text{otherwise.} \end{cases} \tag{17}$$

In the present case we have chosen $a = 3.0$ and $b = 4.5$ and with $L = 2$ we are thus forcing modes with a length scale which is approximately one-tenth of the domain size. Note that since equation (16) depends on time it will have to be recalculated during the simulations.

Due to the direct accessibility to the spectral coefficients of this forcing term equation (16) can be used directly in the simulations with the double periodic code, whereas in the algorithm to compute flows in circular domains the summations have to be evaluated for all the collocation points. As such summations are quite time consuming operations, they are only computed every 10 time steps. We note that interpolating equation (16) onto the circular domain results in a quantity which is not torque-free and therefore the angular momentum will accumulate in course of time. For this reason it is important to remove this (small) contribution from the forcing term. This is achieved by adding a (small) solid body rotation to equation (16). If we omit adding such a contribution we observe a significant spin-up of the flow originating from the accumulated angular momentum entering the system through the forcing as specified by equation (16).

*Figure 5* display the time evolution of the vorticity field using periodic boundary conditions and for $\tau_{diff} = 0.1$. The inverse cascade is clearly observed as the flow organizes into two huge, opposite-signed, monopoles occupying the whole domain. Once these monopoles have been formed they will dominate the evolution, absorbing the energy being pumped into the flow through the forcing, continuously increasing their amplitudes. This process will accelerate when $\tau_{diff}$ increases. Note that the length scale observed in *figure 5* for $T = 1.0$ corresponds approximately to the length scale used in the forcing term.

*Figures 6* and *7* display the time evolution for the bounded (disk) case for two different values of $\tau_{diff}$. In *figure 6* results are displayed for the same value of $\tau_{diff}$ as used in *figure 5*, whereas in *figure 7* plots are shown for the more extreme case of $\tau_{diff} = 100$. Only initially *figure 6* displays the same evolution as the unbounded case. We observe structures with the same length scales as the forcing term (see $T = 2.0$) but quickly the structures start to interact with the boundary and small-scale structures are created. These are injected into the interior of the domain preventing larger structures from emerging (or even destroying larger structures). This turbulent state is thus maintained at a Reynolds number of $Re = 2{,}400$. For higher and lower values of $\tau_{diff}$ we find qualitatively the same kind of evolution as displayed in *figure 6*, e.g. domain filling structures are prevented from emerging due to wall-created small-scale vorticity. This is the case even for nearly static forcing, see *figure 7*, even though short lived structures do emerge (see the flow evolution at $T = 10.0$), but they quickly become unstable and break down into smaller structures. The Reynolds number of the flow in this simulation varies in the range $3{,}000 < Re < 5{,}000$.

Frequently used tools to characterize the flow field are the total kinetic energy and the total enstrophy of the flow as defined by equations (6) and (7), respectively. The time evolution of these two quantities for present simulations can be seen in *figure 8*. In the unbounded case the inverse cascade is again clearly visible (shown for $\tau_{diff} = 0.1$). Energy grows continously in time whereas the corresponding enstrophy quickly settles, at a value of approximately 500. (Similar results are observed for all values of $\tau_{diff}$ with the exception of very large value

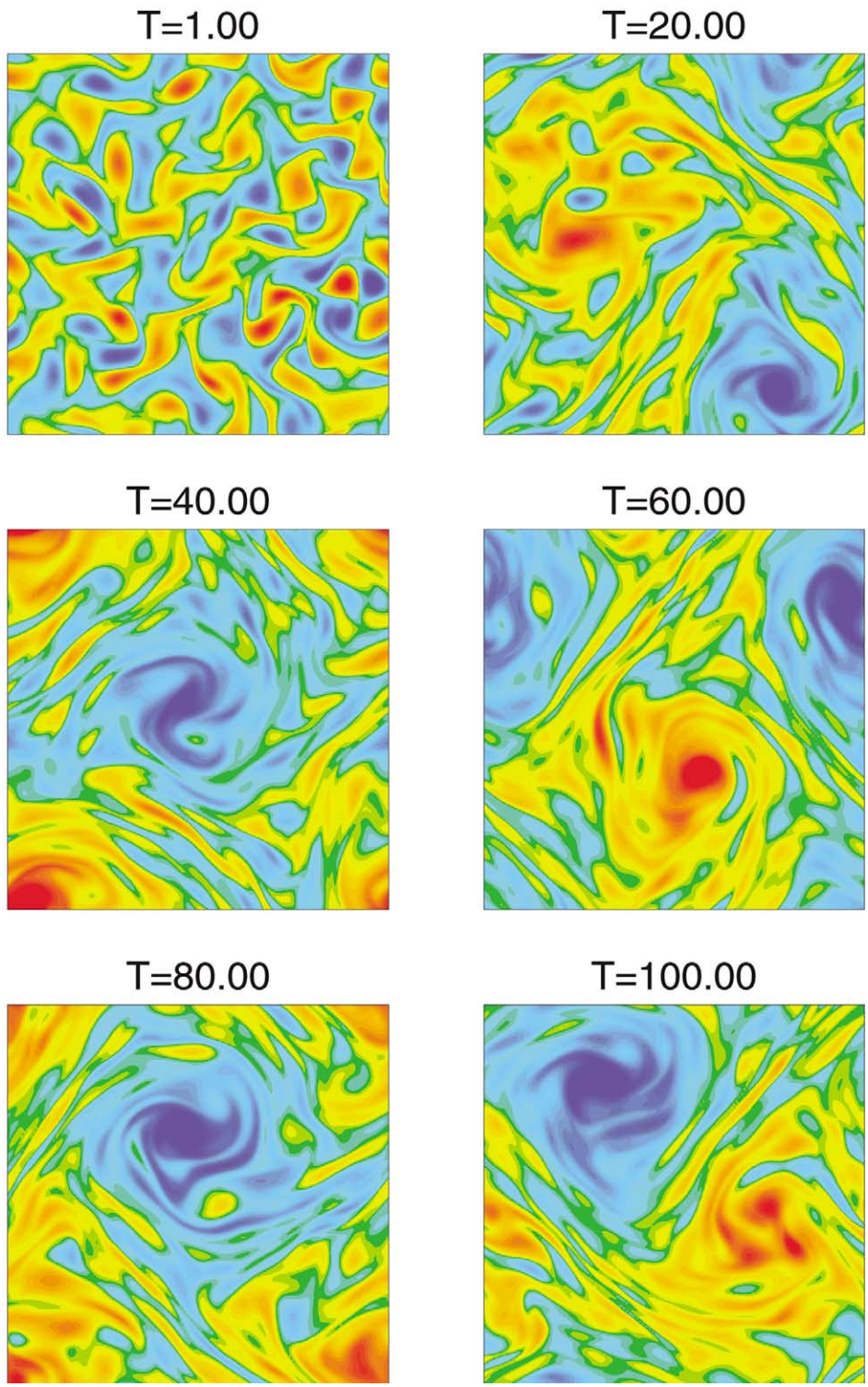


**Figure 5.** The vorticity field of the flow on a double periodic domain using $\tau_{diff} = 0.1$. Red corresponds to positive values, whereas blue corresponds to negative values. In total 30 vorticity levels are displayed with a maximum of $\pm 50$. Spectral resolution $N = M = 256$. The Reynolds number increases from $Re \approx 1{,}000$ for $T = 1.0$ to $Re \approx 5{,}400$ for $T = 100.0$.

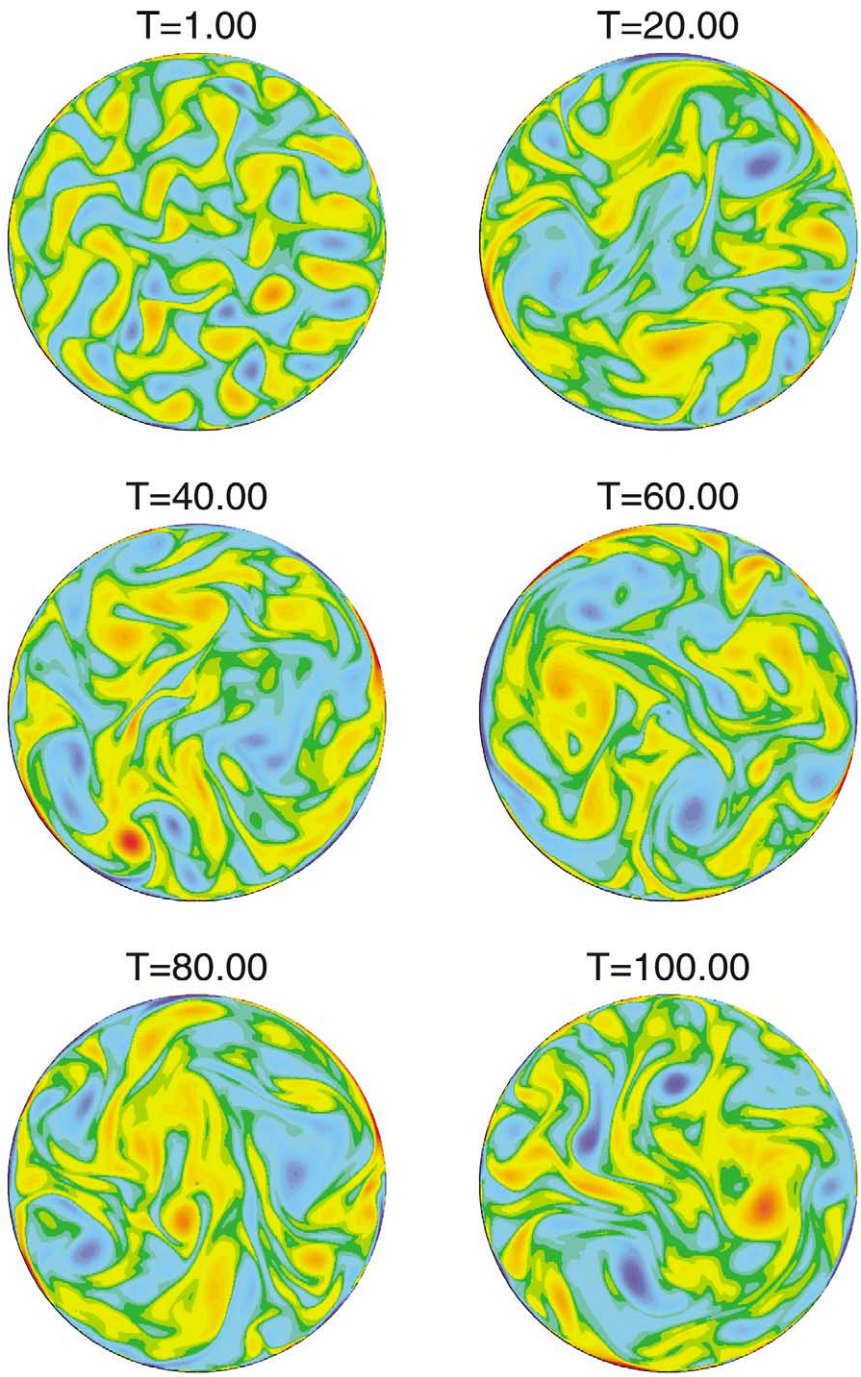


**Figure 6.** The vorticity field of a flow in a circular domain with no-slip boundary conditions using $\tau_{diff} = 0.1$. Red corresponds to positive values, whereas blue corresponds to negative values. In total 30 vorticity levels are displayed with a maximum of $\pm 100$. Spectral resolution $M = 512$ (radially), $N = 512$ (azimuthally). The Reynolds number increases from $Re \approx 1{,}100$ for $T = 1.0$ to $Re \approx 2{,}500$ for $T = 100.0$.

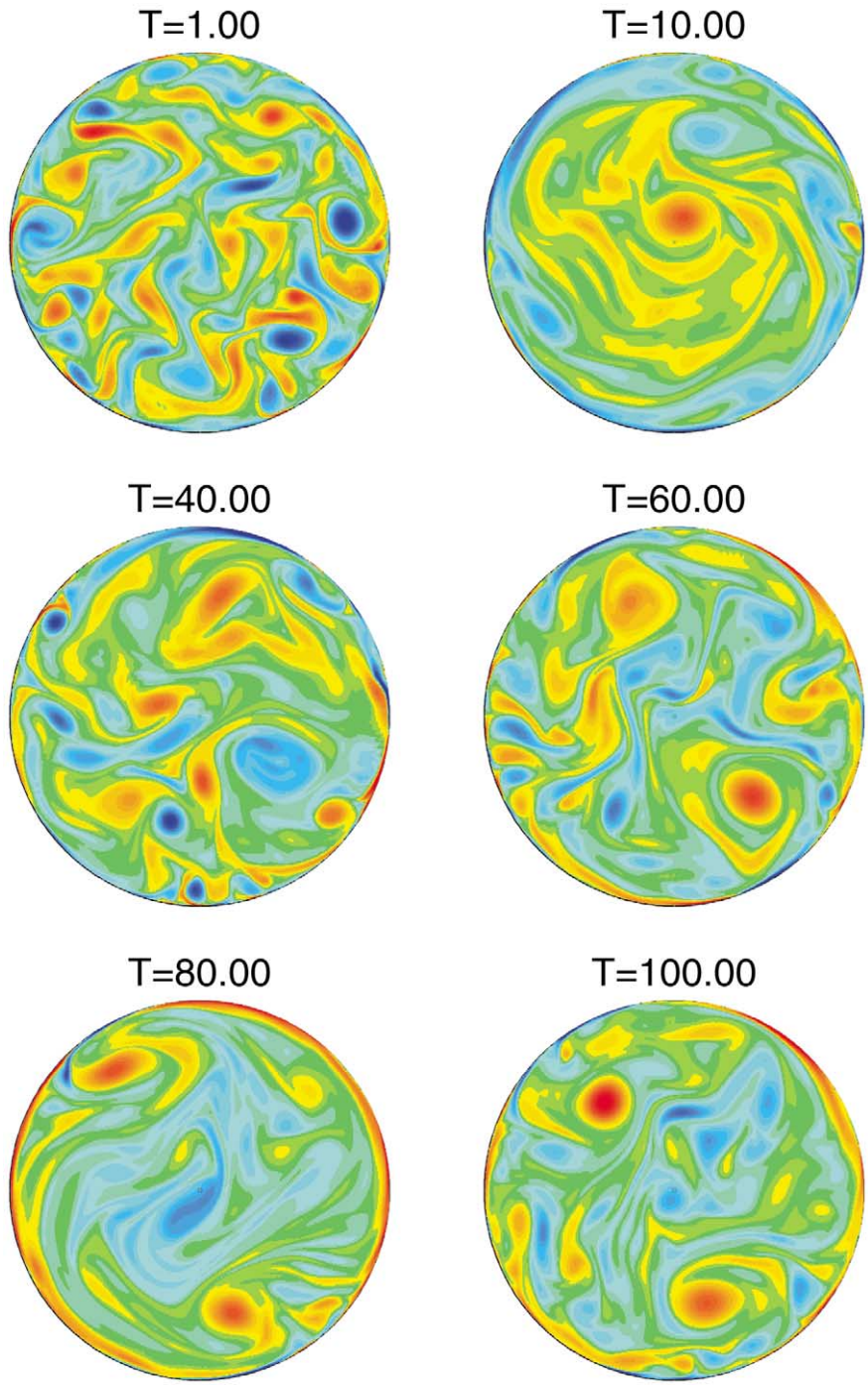


**Figure 7.** The vorticity field of a flow in a circular domain with no-slip boundary conditions using $\tau_{diff} = 100$. Red corresponds to positive values, whereas blue corresponds to negative values. In total 30 vorticity levels are displayed with a maximum of $\pm 150$. Spectral resolution $M = 512$ (radially), $N = 512$ (azimuthally). The Reynolds number increases from $Re \approx 2{,}200$ for $T = 1.0$ to $Re \approx 3{,}500$ for $T = 100.0$.

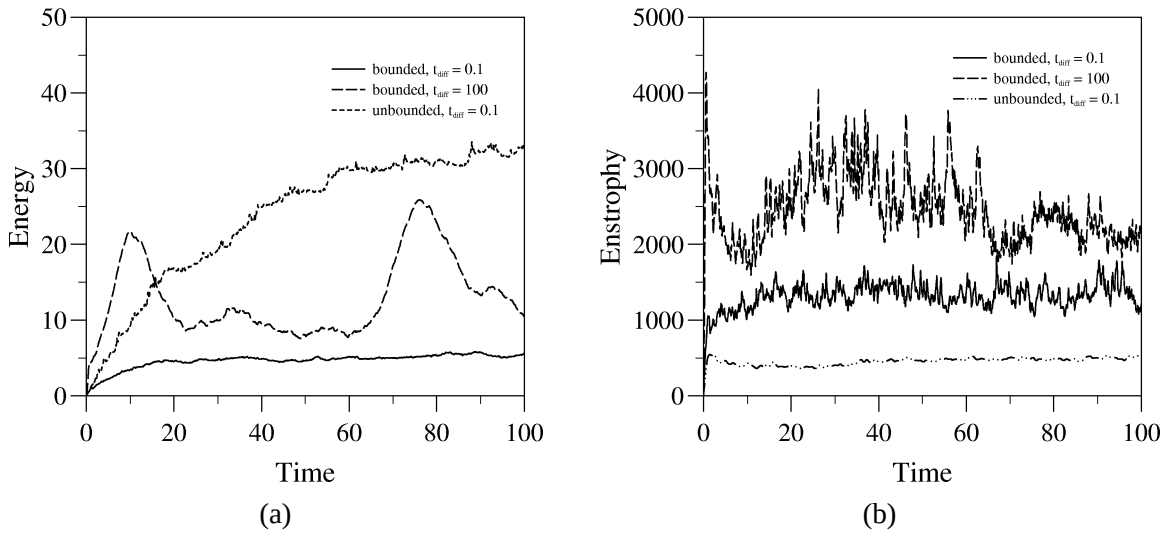


**Figure 8.** Energy (a) and enstrophy (b) evolution of the flow fields displayed in *figures 5* to *7*.

of $\tau_{diff}$. Here self-similar smooth structures can be observed late in the simulations in which case both energy and enstrophy grow rapidly in time.) In present numerical experiments we are pumping energy and enstrophy into a specific part of the spectrum and the enstrophy cascades towards smaller wave numbers where viscous dissipation is the dominant physical process. A stable situation is thus quickly established for the enstrophy. Energy, on the other hand, cascades towards larger wave numbers and it will settle at the largest wave number accessible. Since the kinematic viscosity has virtually no effect in this part of the spectrum energy will simply accumulate there. This is a well-known effect first discussed, for both the 2D Navier–Stokes and the 2D MHD cases, by Hossain et al. [33].

In the corresponding bounded case, e.g. for $\tau_{diff} = 0.1$, we observe a different evolution. The energy settles at a value of 5 and the enstrophy, even though it is strongly fluctuating, settles at a value of approximately 1,400. This enstrophy level is three times larger than computed for the unbounded flow which can be explained by the presence of the boundary layer near the no-slip wall of the circular domain. The vorticity values in the boundary layer are usually very high which affects the enstrophy considerably. It appears that the values of the vorticity in the boundary layer is approximately three times larger than in the interior of the domain and therefore most of the enstrophy is located there. In addition, the creation of small-scale structures near no-slip walls, containing high amounts of enstrophy but small amounts of energy, makes the time evolution quite spiky. This feature is also observed for decaying 2D turbulence in a square domain with no-slip boundaries.

We note that for all values of $\tau_{diff} \leqslant 10$ we find similar behavior for the evolution of both energy and enstrophy. Energy and enstrophy will settle at a constant value, although this value will increase for increasing $\tau_{diff}$. For $\tau_{diff} = 100$ we do observe more variations in the energy evolution with a peak value of 25. This is a larger value than found for smaller $\tau_{diff}$ but it is still a minor effect compared to the unbounded case. There the maximum energy computed in a similar run was nearly 700 (computation up to $T = 18.0$). An important conclusion here is that the presence of no-slip boundaries introduces a quite natural way to remove energy, injected by the forcing, from the flow as can be concluded from the plateau-value in the energy for the bounded case (see *figure 8(a)*). We do not need an artificial sink of energy as usually employed in simulations of forced 2D turbulence with periodic boundary conditions.

The angular momentum for flows in a circular domain is given by

$$L(t) = \int_0^1 \int_0^{2\pi} r u_\theta(\mathbf{r}, t) r \, \mathrm{d}r \, \mathrm{d}\theta = -\frac{1}{2} \int_0^1 \int_0^{2\pi} r^2 \omega(\mathbf{r}, t) r \, \mathrm{d}r \, \mathrm{d}\theta, \tag{18}$$

a relation which is actually identical to the one presented in equation (10). Note that such a relation is not meaningfull for unbounded (periodic) flows, because it is not properly defined. In *figure 9* we have plotted the temporal evolution of the angular momentum for the numerical experiments displayed in *figures 6* and *7*. We have normalised the curve with: $\sqrt{8\pi E(t)/9}$ which is the angular momentum of a flow in solid body rotation with the energy $E(t)$ (equation (6)). (We note that it can readily be shown, with the use of calculus of variations and Lagrange multipliers, that if the energy is kept constant a solid body rotation is the situation which maximises the angular momentum.) For $\tau_{diff} = 0.1$ we observe little change in angular momentum with peak values up to 20% of solid body rotation. Similar results are found for $\tau_{diff} \leqslant 10$. For $\tau_{diff} = 100$ we do observe an angular momentum of the flow which compares rather well with large-scale rotation of the flow (the maximum of $|L(t)|$ corresponds to 85% of solid body rotation). The maximum coincides with the appearance of a large-scale structure but as this structure breaks down the angular momentum decreases again.

An important difference between the bounded square and circular case with regard to the time evolution of $L(t)$ (disregarding the role of forcing for the moment) is the absence of a pressure-induced contribution to the time rate of change of the angular momentum in the latter case. For a circular domain $(\mathbf{r} \cdot \mathrm{d}\mathbf{s})_{\partial D} = 0$, thus

$$\frac{\mathrm{d}L(t)}{\mathrm{d}t} = \nu \oint_{\partial D} \omega(\mathbf{r}, t)(\mathbf{r} \cdot \mathbf{n}) \, \mathrm{d}s = \nu R \oint_{\partial D} \omega(\mathbf{r}, t) \, \mathrm{d}s \tag{19}$$

(with $R$ the radius of the circular domain), and $\mathrm{d}L(t)/\mathrm{d}t$ depends only on the vorticity produced at the no-slip wall (and on the forcing term if present). As a consequence the first term of the right hand side of equation (12) should also be zero. This is indeed the case for flows in a bounded circular domain with radius $R$:

$$\nu \oint_{\partial D} r^2 \frac{\partial \omega}{\partial n} \, \mathrm{d}s = \nu R^2 \oint_{\partial D} \frac{\partial \omega}{\partial n} \, \mathrm{d}s = R^2 \frac{\mathrm{d}\Gamma}{\mathrm{d}t} = 0, \tag{20}$$

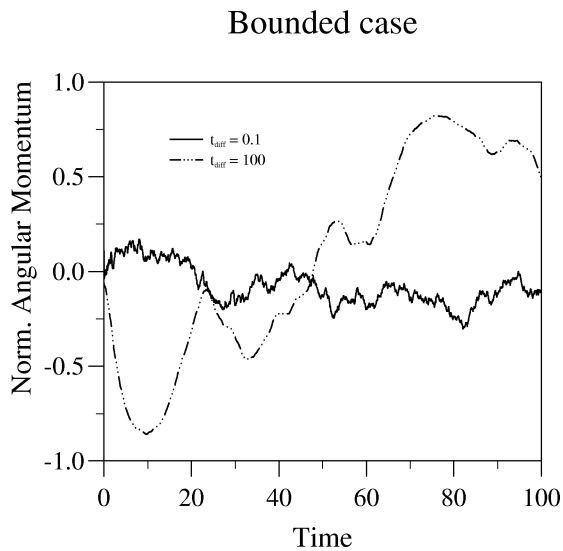


**Figure 9.** Normalised angular momentum evolution of the flow for the circular domain displayed in *figures 6* and *7*.

with $\Gamma$ the total circulation of the flow, which is constant (actually equal to zero) for bounded flows with stationary walls. As mentioned in section 4, in a non-circular domain, e.g. where $(\mathbf{r} \cdot \mathrm{d}\mathbf{s})_{\partial D} \neq 0$, $\mathrm{d}L(t)/\mathrm{d}t$ will be dominated by the normal vorticity gradient integrated over the boundary, whereas the total shear stress along the boundary is of minor importance. The relatively small values of $L(t)$ observed in *figure 9* can be seen as a result of the absence of the term containing the pressure contribution, and one can generally conclude that spin-up in a circular domain will very likely be absent (see also [30,31]). Note that decaying 2D turbulent flows containing an appreciable amount of angular momentum in the initial flow field behave somewhat different [34,31].

## 6. Conclusions

A summary of fascinating phenomena of 2D turbulence in bounded domains has been presented. For freely evolving 2D turbulence these phenomena concern the non-trivial behaviour of 1D spectra near boundaries, the different behaviour of the evolution of vortex statistics, and the spontaneous spin-up of the flow during the decay of turbulence. The latter process has been discussed in more detail and it has been shown that this process occurs for low and high initial integral-scale Reynolds numbers. The presence of spontaneous spin-up is also independent of the kind of initial conditions of the flow. Another set of numerical experiments concern forced 2D turbulence in circular containers.

The main conclusions of this part are that the circular boundary prevents larger scale structures from emerging in the flow as small-scale structures are continuously created at the boundary and are subsequently injected into the interior of the flow, maintaining the turbulent flow field. This situation is quite different from the periodic case, where one always observe the inverse cascade in which energy accumulates in the largest scale possible (two monopolar structures). Additionally, it is not necessary to include an artificial energy sink for the bounded flows in order to avoid unbounded growth of the kinetic energy of the flow: the no-slip boundaries serve as a sufficient sink of energy. Concerning spontaneous spin-up the circular domain is special as only the total shear stress along the boundary will contribute to the change of angular momentum. In these simulations we only observe a small change in angular momentum. In the square domain, on the other hand, the change of angular momentum will be dominated by the normal vorticity gradient integrated over the boundary, and spontaneous spin-up is therefore more likely to occur.

An important aspect which has to be studied for decaying and for forced 2D turbulence is the precise role of the no-slip boundaries as vorticity source (e.g. the production of vorticity and normal vorticity gradients as function of the Reynolds number) and the role of the boundary layers on the flow dynamics, especially in the limit of high Reynolds numbers. This requires, however, an enormous computational effort due to large amount of necessary CPU-time. Nevertheless, such an investigation would be worthwhile to carry out.

## Acknowledgements

One of us (H.J.H.C.) is grateful for support by the European Science Foundation (ESF-TAO/1998/13). Part of this work was sponsored by the Stichting Nationale Computerfaciliteiten (National Computing Facilities Foundation, NCF) for the use of supercomputer facilities, with financial support from the Nederlandse Organisatie voor Wetenschappelijk Onderzoek (Netherlands Organization for Scientific Research, NWO).

## References

[1] Kraichnan R.H., Montgomery D., Two-dimensional turbulence, Rep. Prog. Phys. 43 (1980) 547–619.
[2] Kraichnan R.H., Inertial ranges in two-dimensional turbulence, Phys. Fluids 10 (1967) 1417–1423.
[3] Batchelor G.K., Computation of the energy spectrum in homogeneous two-dimensional turbulence, Phys. Fluids Suppl. II 12 (1969) 233–239.
[4] Lilly D.K., Numerical simulation of two-dimensional turbulence, Phys. Fluids Suppl. II 12 (1969) 240–249.
[5] Frisch U., Sulem P.L., Numerical simulation of the inverse cascade in two-dimensional turbulence, Phys. Fluids 27 (1984) 1921–1923.
[6] Legras B., Santangelo P., Benzi R., High-resolution numerical experiments for forced two-dimensional turbulence, Europhys. Lett. 5 (1988) 37–42.
[7] Borue V., Inverse energy cascade in stationary two-dimensional homogeneous turbulence, Phys. Rev. Lett. 72 (1994) 1475–1478.
[8] Santangelo P., Benzi R., Legras B., The generation of vortices in high-resolution, two-dimensional decaying turbulence and the influence of initial conditions on the breaking of self-similarity, Phys. Fluids A 1 (1989) 1027–1034.
[9] Brachet M.E., Meneguzzi M., Sulem P.L., Small-scale dynamics of high Reynolds-number two-dimensional turbulence, Phys. Rev. Lett. 57 (1986) 683–686.
[10] Matthaeus W.H., Montgomery D., Selective decay hypothesis at high mechanical and magnetic Reynolds numbers, Ann. NY Acad. Sci. 357 (1980) 203–222.
[11] McWilliams J.C., The emergence of isolated coherent vortices in turbulent flow, J. Fluid Mech. 146 (1984) 21–43.
[12] Matthaeus W.H., Stribling W.T., Martinez D., Oughton S., Montgomery D., Selective decay and coherent vortices in two-dimensional incompressible turbulence, Phys. Rev. Lett. 66 (1991) 2731–2734.
[13] Leith C.E., Minimum enstrophy vortices, Phys. Fluids 27 (1984) 1388–1395.
[14] Carnevale G.F., McWilliams J.C., Pomeau Y., Weiss J.B., Young W.R., Evolution of vortex statistics in two-dimensional turbulence, Phys. Rev. Lett. 66 (1991) 2735–2737.
[15] Carnevale G.F., McWilliams J.C., Pomeau Y., Weiss J.B., Young W.R., Rates, pathways, and end states of nonlinear evolution in decaying two-dimensional turbulence: Scaling theory versus selective decay, Phys. Fluids A 4 (1992) 1314–1316.
[16] Cardoso O., Marteau D., Tabeling P., Quantitative experimental study of the free decay of quasi-two-dimensional turbulence, Phys. Rev. E 49 (1994) 454–461.
[17] Hansen A.E., Marteau D., Tabeling P., Two-dimensional turbulence and dispersion in a freely decaying system, Phys. Rev. E 58 (1998) 7261–7271.
[18] Weiss J.B., McWilliams J.C., Temporal scaling behavior of decaying two-dimensional turbulence, Phys. Fluids A 5 (1993) 608–621.
[19] Clercx H.J.H., Maassen S.R., van Heijst G.J.F., Spontaneous spin-up during the decay of 2D turbulence in a square container with rigid boundaries, Phys. Rev. Lett. 80 (1998) 5129–5132.
[20] Clercx H.J.H., van Heijst G.J.F., Energy spectra for decaying 2D turbulence in a bounded domain, Phys. Rev. Lett. 85 (2000) 306–309.
[21] Clercx H.J.H., Nielsen A.H., Vortex statistics for turbulence in a container with rigid boundaries, Phys. Rev. Lett. 85 (2000) 752–755.
[22] Clercx H.J.H., A spectral solver for the Navier–Stokes equations in the velocity-vorticity formulation for flows with two nonperiodic directions, J. Comput. Phys. 137 (1997) 186–211.
[23] Orszag S.A., Numerical methods for the simulation of turbulence, Phys. Fluids, Suppl. II 12 (1969) 250–257.
[24] Chasnov J.R., On the decay of two-dimensional homogeneous turbulence, Phys. Fluids 9 (1997) 171–180.
[25] Clercx H.J.H., Maassen S.R., van Heijst G.J.F., Decaying two-dimensional turbulence in square containers with no-slip or stress-free boundaries, Phys. Fluids A 11 (1999) 611–626.
[26] Bergeron K., Coutsias E.A., Lynov J.P., Nielsen A.H., Dynamical properties of forced shear layers in an annular geometry, J. Fluid Mech. 402 (2000) 255–289.
[27] Pointin Y.B., Lundgren T.S., Statistical mechanics of two-dimensional vortices in a bounded container, Phys. Fluids 19 (1976) 1459–1470.
[28] Ting A.C., Chen H.H., Lee Y.C., Exact vortex solutions of two-dimensional guiding-center plasmas, Phys. Rev. Lett. 53 (1984) 1348–1351.
[29] Ting A.C., Chen H.H., Lee Y.C., Exact solutions of a nonlinear boundary value problem: the vortices of the two-dimensional sinh-Poisson equation, Physica D 26 (1987) 37–66.
[30] Li S., Montgomery D., Decaying two-dimensional turbulence with rigid walls, Phys. Lett. A 218 (1996) 281–291.
[31] Maassen S.R., Clercx H.J.H., van Heijst G.J.F., Decaying quasi-2D turbulence in a stratified fluid with circular boundaries, Europhys. Lett. 46 (1999) 339–345.
[32] Torres D.J., Coutsias E.A., Pseudospectral solution of the two-dimensional Navier–Stokes equations in a disk, SIAM J. Sci. Comp. 21 (1999) 378–403.
[33] Hossain M., Matthaeus W.H., Montgomery D., Long-time states of inverse cascades in the presence of a maximum length scale, J. Plasma Phys. 30 (1983) 479–493.
[34] Li S., Montgomery D., Jones W.B., Inverse cascades of angular momentum, J. Plasma Phys. 56 (1996) 615–639.